Journal of Magnetism and Magnetic Materials 407 (2016) 291–298

Contents lists available at ScienceDirect

Journal of Magnetism and Magnetic Materials

journal homepage: www.elsevier.com/locate/jmmm

Magnetocapacitance effect in ferromagnetic $LiNbO_3$ nanoparticles

Carlos Díaz-Moreno [a], Jorge Lopez [a], Jesus González-Hernández [b], Roberto Escudero [c], Jesus L. Heiras [d], Miguel J. Yacamán [e], Juan Mendez-Nonell [f], Abel Hurtado-Macias [f,*]

[a] Department of Physics of University of Texas at El Paso, 500W. University Ave, El Paso, TX 79968, USA
[b] Centro de Ingeniería y Desarrollo Industrial, Santiago de Querétaro, 76130 Qro., México
[c] Universidad Nacional Autónoma de México, Departamento de Materia Condensada y Criogenia, Av. Universidad 3000, Coyoacán, México D. F. 04510, México
[d] Universidad Nacional Autónoma de México, Centro de Nanociencias y nanotecnología, Km 107 Carretera Tijuana-Ensenada, Ensenada, B.C. 22860, México
[e] Department of Physics and Astronomy, University of Texas at San Antonio, One UTSA Circle, San Antonio, TX 78249, USA
[f] Centro de Investigación en Materiales Avanzados S.C., Laboratorio Nacional de Nanotecnología, Miguel de Cervantes 120, Complejo Industrial, Chihuahua, Chihuahua Apdo. Postal 31109 México

ARTICLE INFO

Article history:
Received 25 September 2015
Received in revised form
25 December 2015
Accepted 4 January 2016
Available online 4 February 2016

Keywords:
Lithium niobate
Nanoparticles
Ferroelectric
Ferromagnetic
Magnetocapacitance
Multiferroic

ABSTRACT

Magnetocapacitance and magnetization behavior as a function of reduction heat treatment at 650 °C and 900 °C in a 5%H_2–Ar atmosphere on $LiNbO_3$ nanocrystalline are reported. There is a change of intrinsic dielectric constant (κ) from 822 to 860 produced by spin polarization using an external magnetic field. The Raman, X-ray photoelectron spectroscopy and electron paramagnetic resonance spectroscopy, indicate vibration mode changes localized at Nb–O bonds in the octahedron NbO_6, shifts in the binding energy of the electronic structure of ions of niobium (3*d*) and the oxygen (1*s*). It is due to the oxygen vacancies caused by reduction heat treatment process. Moreover there is ions redistribution of Nb^{+3}, $Nb^{+4}$and Nb^{+5} at the surface of the nanoparticles.

1. Introduction

The search for better multiferroic materials had occurred in the past 10 years as indicated by Fiebig [1], due to important position in the development of several technological electronic applications [2]. Perovskite structure types ABO_3 (i.e., $PbTiO_3$, $BaTiO_3$, Pb(Zr,Ti)O_3 and $LiNbO_3$) seems to be an ideal candidate material for nonlinear optical applications [3]. The understanding of the multiferroic phase can be achieved through measurements in which an external magnetic field is applied. Coey et al. [4] presented ferromagnetism in TiO_2 by implanting Fe cations in films as prepared by pulse-laser deposition. Hysteresis curves determined that 1–2% of the sample possessed magnetic order with about 2.2 μ_B per iron atom. A theoretical hypothesis about the origin of ferromagnetism in $LiNbO_3$ was made by Weis et al. [5], attributing the magnetic order to the addition of dopants into $LiNbO_3$ structure, which provoked changes in the electronic structure of Li–Nb–O. This was in agreement with Kong et al. [6] when Ni^+, Fe^+ or Mn^+ and Co^+ ions were implanted into $LiNbO_3$. Song et al. [7], reported simultaneous room temperature ferromagnetism and ferroelectricity unambiguously observed in Cobalt implanted $LiNbO_3$ (Co:$LiNbO_3$) thin films (grown onsilicon substrates) with the transition temperatures of thin films at T_c (~540 K) and of T_E (~610 K), which is a fairly high ferroelectric transition temperature. These observations suggest that Co:$LiNbO_3$ opens the possibility for multiferroic device applications. The magneto-capacitance effect occurs in multiferroic materials due to spin polarization by external magnetic fields and it was attributed mainly to an intrinsic property in its dielectric constant, Kimura et al. [8]. As well as reported that the change in the dielectric constant due to the magnetostriction is near 4×10^{-3}% when measured in external field of 70 kOe at 110 K in $BiMnO_3$ material. On the other hand, Hemberger et al. [9] pointed out that charge carriers do not have time to respond to high frequency fields, thus, a measured capacitance value will correspond to two insulating capacitors when connected in series. Previous investigations [10] made by our group in lithium niobate nanoparticles prepared by solid state mechanical milling reaction, resulted in a measured a magnetic remanence of $M_r = 0.35 \times 10^{-3}$ emu/g and in a coercive field of $H_c = 0.75$ kOe confirming that it possessed multiferroic properties. In perovskite materials the Raman technique is suitable to the determination of vibrational frequencies; particularly features such as disorder, interaction with excess carriers and quantum

* Corresponding author.

http://dx.doi.org/10.1016/j.jmmm.2016.01.010
0304-8853/

confinement were investigated by Dobal et al. [11] aimed to determine both ionic charge and radii induced changes due to atomic substitution in $PbTiO_3$ thin films, as well in $BaTiO_3$ (BTO), and observed an induced linear variation of the ferroelectric transition temperature. Electron paramagnetic resonance (EPR) is the most powerful spectroscopic method available to study ferroelectromagnetics systems ABO_3 type with high dielectric-κ constant. Alvarez et al. [12–15] reported several studies in the compounds $Pb(Fe_{1/2}Nb_{1/2})O_3$, $Pb(Fe_{0.5}Ta_{0.5})O_3$, $Pb(Fe_{1-x}Nb_x)O_3$ and $Ni_{0.35}Zn_{0.65}Fe_2O_4$ in which they determine the nature of magnetic phase, electric phase, structural information and symmetry of the incorporated transition metal ion providing valuable information about the nature of magnetic ordering in these multiferroics materials.

In this work, we present the results of studying the magnetic and magnetocapacitance effect by measuring magnetization curves at 300 K on ferromagnetic lithium niobate nanoparticles single phase subjected to an external field, aimed to investigate the effect of reduction heat treatment. Three different samples were used, one without reduction heat treatment and the other two with reduction heat treatment at 650 °C and 900 °C. Furthermore, samples were characterized by conventional spectroscopy techniques such as Raman, XPS, EPR and Corrected Scanning Transmission Electron Microscopy (STEM) to determine modes of vibration, binding energies, the natures of magnetic ions and structural aspects, respectively.

2. Experimental details

2.1. $LiNbO_3$ nanoparticle preparation

Using 0.6525 gm of lithium carbonate (Li_2CO_3) and 2.3474 gm of niobium oxide (Nb_2O_5) with high purity (99.99%) commercially available from Alfa Aesar as precursors, a mixture is produced by mechanical milling with a nylon vial and zirconia ceramic balls by high energy ball milling (SPEX Series 8000M) with mixture/balls relation of 0.1. Milling time used was 300 minutes, followed by a heat treatment of calcination at 650 °C in a Thermolite 2136 in air atmosphere to obtain the $LiNbO_3$ nanoparticles, according to the following solid-state reaction:

$$Nb_2O_5(s) + Li_2CO_3(s) \rightarrow 2LiNbO_3(s) + CO_2(gas) \quad (1)$$

After obtained $LiNbO_3$ nanoparticles a second reduction heat treatment (RHT) process were performed at 650 °C and 900 °C in a 5%H_2–Ar atmosphere to obtain ferromagnetic nanoparticles caused by oxygen vacancies, for more details see reference [16].

2.2. Experimental of structural characterization of the $LiNbO_3$ nanoparticles with a without RHT by HRTEM, Raman Spertroscopy and X-ray photoelectron Spectroscopy.

High resolution images were obtained using a JEOL ARM (200F) microscope, operating at 200 kV, equipped with a Cs corrector (CEOS GmbH) and a FEG-STEM/TEM unit. The high angle annular dark field (HAADF) probe size was set to 0.095 nm and a current of 23.2 pA was used for bright field imaging. Condenser lens aperture sizes were set to 40 μm. A camera length (CL) of 8 cm/6 cm and collection angle of 68–280 mrad/90–270 was chosen in order to eliminate contributions from unscattered beams.

Raman Spectroscopy was made using a Micro Lab RAM HR model (Lexc=632.8 nm), within a range from 100 to 1000 cm^{-1}, with a 14 mW laser excitation power, using a 100× objective and an aperture of ~1 μm. On the other hand, XPS spectra were obtained with a JEOL JPS-9200 spectrometer, equipped with a source of magnesium X-rays (MgKα) (1253.6 eV) at 200 W, with a 3 mm^2 analysis area, at an ultrahigh vacuum (about 10^{-8} Torr). The spectra were analyzed using SpecSurf® package. All spectra obtained were corrected using a carbon signal (C1s) at 284.5 eV. The Shirley method was used for extracting the background necessary for curve fitting was used.

2.3. EPR spectroscopy

Electron paramagnetic resonance measurements were performed with a JEOL JES-RES 3X spectrometer operating at X-band (8.8–9.8 GHz) with 100 kHz of modulation on the applied dc magnetic field (H_{dc}). H_{dc} could be varied from 0 to 5000 G. The EPR spectra were recorded at 300 K.

2.4. Magnetization and magnetocapacitance measurements of the $LiNbO_3$ nanoparticles with a without RHT

Magnetization measurements were performed using a Physical Properties Measurements (PPMS) equipment model 9 T (Quantum Design) with a Vibrating Sample Magnetometer. Measurements were performed at 300 K. On the other hand, the magneto capacitance effect was measured using an Agilent E4980A equipment, in a frequency range from 20 Hz to 2 MHz in conjunction with precision LCR meter and a VersaLab 3 T (Quantum Design) vibrating sample magnetometer. The capacitance measurements were made using parallel plate formula approximation. Samples of $LiNbO_3$ nanocrystals without the RHT and with RHT at 650 °C and 900 °C on cylinder shape pellets (6.15×10^{-6} m^2 of area and 1 mm thick.) Wires were attached with silver paint to make contact with the gold electrodes on opposing faces of the pellets. Samples were first subjected to a nominal ac voltage of 0.5 μV at angular frequencies of 500 Hz, 1 kHz, 10 kHz, 50 kHz, 100 kHz, 250 kHz, 500 kHz, 750 kHz and 1 MHz. After measuring the capacitance samples were subjected to an external magnetic field which varied from 1 kOe to 30 kOe in order to observe a magnetocapacitance effect. Measurements were performed at room temperature.

3. Results and discussion

3.1. Structural aspects by cs- corrected scanning electron microscope

Using Cs-corrected high resolution transmission electron microscopy in scanning mode, it was possible to determine both structural and morphological aspects for RHT and non-RHT $LiNbO_3$ samples. A small amount of sample powder was dispersed in ethanol using an ultrasonic bath and then one drop of the solution was deposited into a silicon-carbide 200-mesh TEM grid and dried at room temperature. Mono-dispersed sheets of $LiNbO_3$ were observed in sample without RHT as reported by Díaz-Moreno et al. [17], opposed to the well-formed spherical shape nanoparticles for sample with RHT at 650 °C and 900 °C as shown in Fig. 1(a) and (b). The formation of spherical shape nanoparticles are attributed to the reduction heat treatment, which also causes some structural defects, since nanoparticles were unstable under observation, which in most cases caused diffusion of atoms near the surface. A STEM measurement allows us to conclude that RHT plays a significant role in the formation of spherical shaped nanoparticles.

3.2. Magnetometry analysis of the $LiNbO_3$ nanoparticles with a without RHT

After the calcination process at 650 °C one sample was kept and another two were subjected to an additional reduction heat treatment (RHT) at 650 °C and 900 °C respectively, both in a 5%

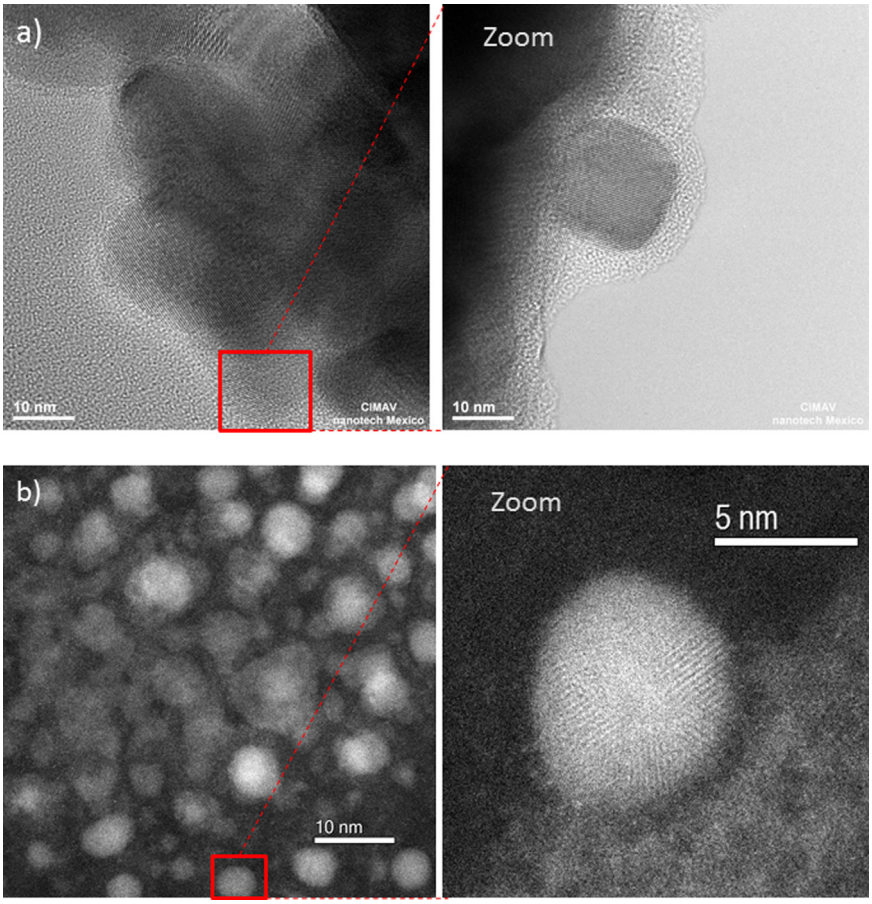

Fig. 1. Dark field and Bright field STEM images corresponding to $LiNbO_3$ with RHT at (a) 650 °C and (b) 900 °C.

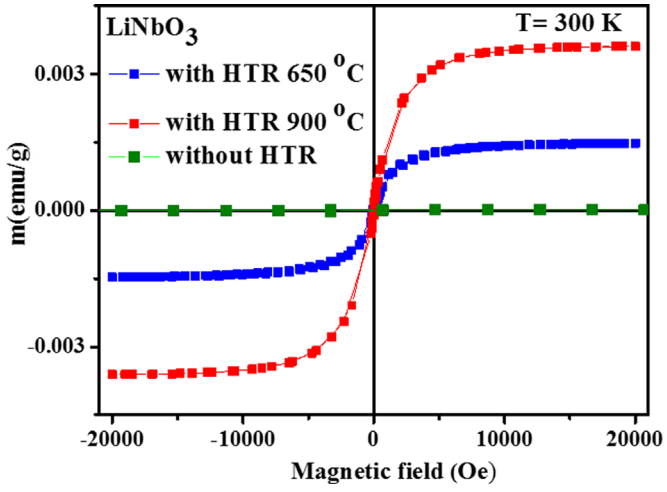

Fig. 2. Magnetization curves measured at external field 9 T at 300 K for two different reduction heat treatment samples 650 °C and 900 °C in comparison without RHT.

H_2–Ar atmosphere for 20 min. A gray coloration was observed in comparison with white powder before the RHT process. The three samples were subjected to magnetization measurements at 9 T external field at room temperature. The hysteresis loop observed for all samples are shown in Fig. 2. This magnetic behavior is typical of the new room temperature ferromagnetism found in defect ridden oxides, explained with defect-based models including the inhomogeneous nature of magnetism in magnetic regions rich in defects, which tend to concentrate at interfaces and grain boundaries [4]. Such behavior is different from superparamagnetism, where the isothermal measurement shows no hysteretic effects when taken at different temperatures, and of course in that case if the particle is small than the wall thickness there is no hysteresis and the different measurements will be superpose when plotted as function of H/T [16]. For the sample with RHT at 650 °C with a mass of 24.3 mg and magnetic moment of 7.53×10^{-4} emu, taking into account the mass density and unit cell volume of $LiNbO_3$ as 4.65 g/cm^3 and 335.9×10^{-24} cm^3, a magnetic moment per unit cell of 5.24×10^{-3} μ_B and a magnetic moment per formula unit of 8.73×10^{-4} μ_B have been calculated. In the same way for the sample with RHT at 900 °C the momentum magnetic was 2.3×10^{-3} emu, therefore magnetic moment per formula unit of 3.5×10^{-3} μ_B. In these results we can conclude that in the sample with RHT at 900 °C there is a higher magnetic effect caused by oxygen vacancies than the sample with RHT at 650 °C. On the other hand, it is evident that the sample which was not subjected to the RHT process is nonmagnetic. To get a deeper insight of the of electronic states, mainly at the octahedral NbO_6 site, both of heat treatment reduction samples were subjected to Raman, XPS and EPR spectroscopy measurements, results which will be discussed in the next sections.

3.3. *Raman and X-ray photoelectron spectroscopy analysis of the $LiNbO_3$ nanoparticles with a without RHT.*

The octahedral site NbO_6 where the polarization occurs to produce the ferroelectric phase of the $LiNbO_3$, thus it is suitable for sample under calcination process condition not to suffer voids (oxygen vacancies) near surface that causes small changes in Raman spectra, as presented in Fig. 3), in close agreement to spectra

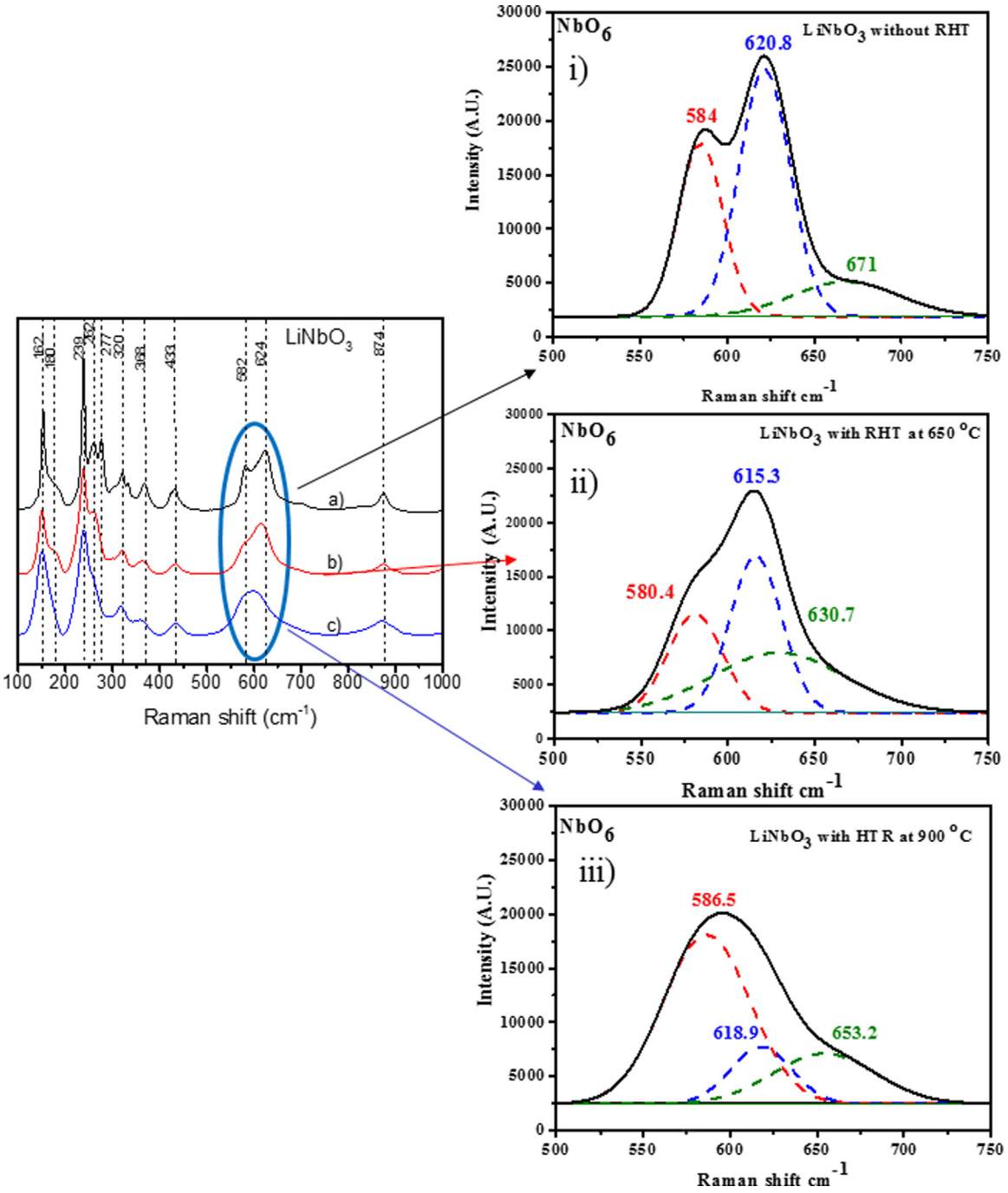

Fig. 3. Vibration modes obtained by Raman techniques at room temperature. (a) Without RHT, (b) and (c) with RHT at 650 °C and 900 °C, respectively.

Table 1
Raman bands for Not RHT, 650 °C and 900 °C RHT on $LiNbO_3$ nanoparticles.

Raman shift (500–750 cm^{-1}) NBO_6	Not RHT	650 °C	900 °C
1	584	580.4	586.5
2	620.8	615.3	618.9
3	671	630.7	653.2

as reported before by Repelin et al. vibration modes located at 152, 180, 239, 262, 277, 320, 333, 368, 433, 582, 610, 620 and 874 cm^{-1} correspond to lithium niobate ferroelectric phase which was not reduction heat treatment after calcination [18]. New vibration modes are observed for lithium–oxygen bonds at octahedral LiO_6 (black plot respect to the red and blue) for samples with RHT at 650 °C (Fig. 3(b)) and 900 °C (Fig. 3(c)) located at 262, 277 and 320 cm^{-1}, corresponding Li–O atoms diffusion due to the reduction heat treatment. On other hand, vibration modes at 615.3 cm^{-1} (with RHT at 650 °C) and 618.9 cm^{-1} (with RHT at 900 °C) correspond to $A_1[TO_4]$ vibration mode associated with the loss of symmetry of oxygen octahedral site NbO_6,caused during the RHT process. The inset of Fig. 3(i), (ii) and (iii), presents Raman deconvolution ranging from 500 to 750 cm^{-1}, which is clearly linked to octahedron NbO_6 vibration modes which are strongly associated with the magnetic properties of the ferromagnetic phase of the $LiNbO_3$. Table 1 summarizes the positions of the Raman bands in the 500–750 cm^{-1} range for Nb–O bonds of the NbO_6 octahedron without RHT and with RHT at 650 °C and at 900 °C.

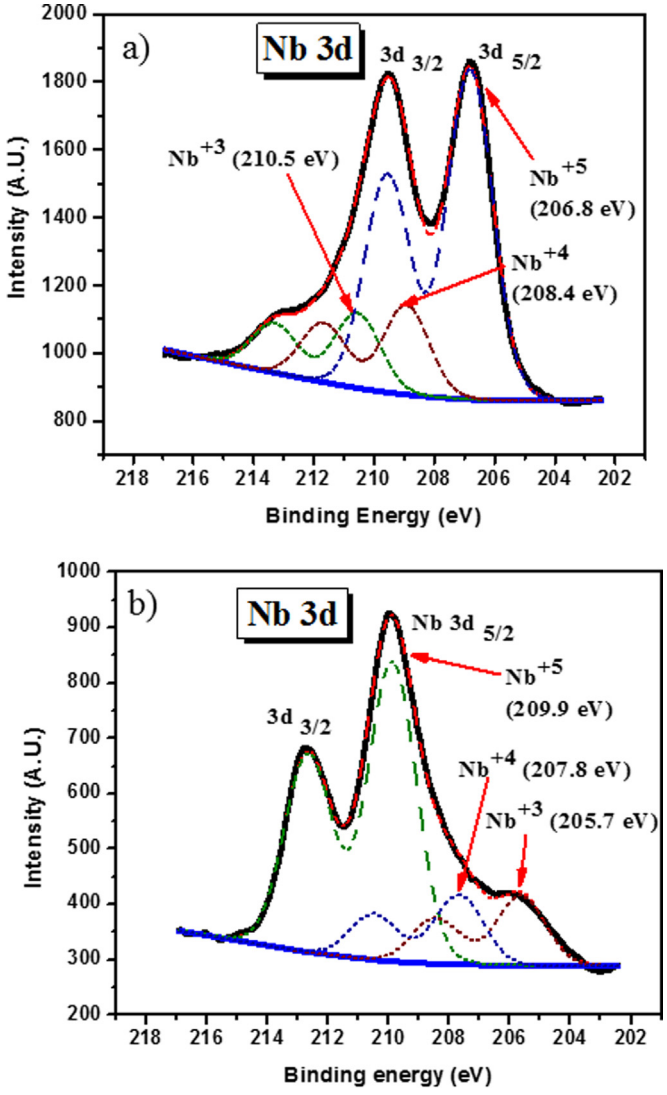

Fig. 4. Binding energies of Nb 3*d*-orbital for surface of $LiNbO_3$ nanoparticles; (a) without reduction heat treatment and (b) with reduction heat treatment at 900 °C.

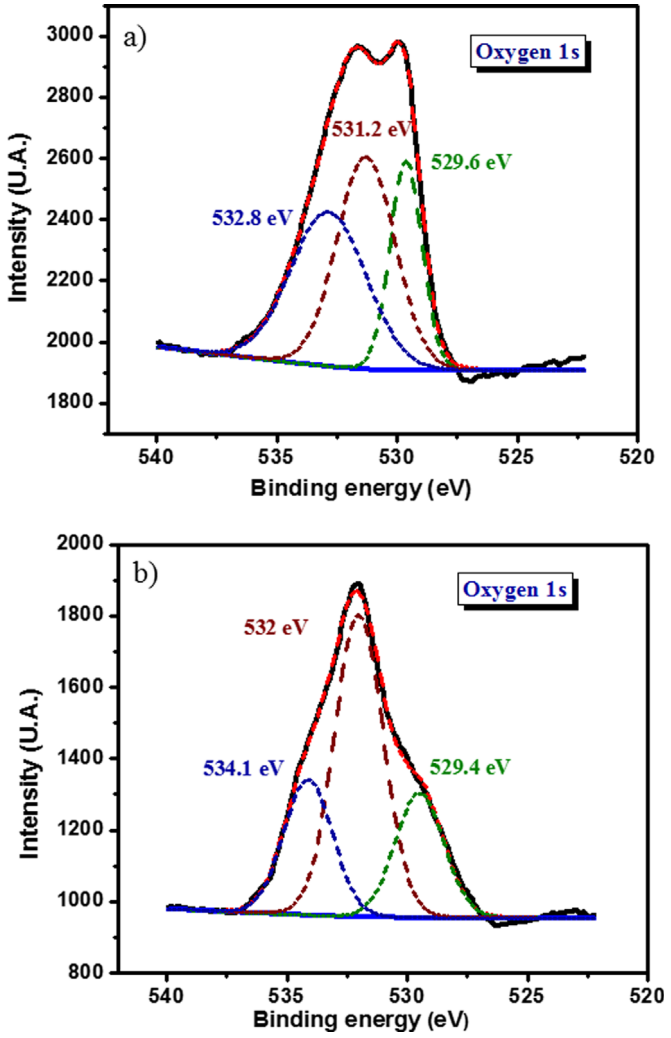

Fig. 5. Binding energies of Oxygen 1*s*-orbital; (a) without RHT and (b) with RHT at 900 °C.

Moreover, XPS measurements, Figs. 4 and 5, show binding energy signals for Nb 3*d* and O 1*s* which correspond to various defects concentration at the surface.

Fig. 4(a) corresponds to the non-reduction heat treated sample showing binding energies of the 3*d*-orbital that are 206.8 eV, 208.4 eV and 210.5 eV, ascribed to Nb^{5+}, Nb^{4+} and Nb^{3+} respectively. Moreover, the sample with RHT at 900 °C in (Fig. 4(b)) binding energies are 209.9 eV, 207.8 eV and 205.7 eV, ascribed to Nb^{5+}, Nb^{4+} and Nb^{3+}. The shifts of the binding energies come from regions with high concentration of oxygen voids which are mainly produced during the RHT [19]. On the other hand, in Fig. 5 (a) the binding energies of 529.6 eV, 531.2 eV and 532.8 eV correspond to the sample with no RHT. On the others side Fig. 5(b), correspond to RHT at 900 °C sample binding energies show at 529.4 eV, 532 eV and 534.1 eV are from oxygen 1*s* orbital binding energies. This provides direct evidence of oxygen diffusion near the surface of $LiNbO_3$ nanoparticles during RHT. These signals are may be ascribed to the loss of oxygen fallowed by the diffusion of lithium in the nanoparticles surface. One observes a binding energy shift; similar findings has been presented by Tabata et al. in $LiNbO_3$ thin films [20].The signal at 529.4 eV is associated with the natural network of $LiNbO_3$, 532 eV signal is associated with the absorption of hydroxyl group (–OH) and signal 534.1 eV is associated with adsorption of oxygen by chemical reduction (in this case, associated with oxygen vacancies (O*) created during RHT, proving generation of oxygen vacancies near surface of the nanoparticle, as reported by Courths et al. [21].

3.4. EPR spectroscopy

Electron paramagnetic resonance (EPR) measurements are presented, because this technical contribute significantly to the understanding the role of paramagnetic ions $LiNbO_3$ nanocrystals in representative sample with RHT at 900 °C which was most significant results compared with the RHT at 650 °C sample. Fig. 6 (a) shows the EPR signal (d*P*/d*H* vs magnetic field) at room temperature for the RHT at 900 °C sample. Two signals are observed. The first corresponds to a resonance field of 3500 G and a width of 60 G; it can be attributed to oxygen vacancies in crystalline structure. Each vacancy contains a trap of two electrons in an analogy with earlier studies of similar defects discussed in a paper by Sweeney et al. [19]. The second signal shows Lorenz type symmetric mode absorption with a 1500 G line width and a resonance field of 3000 G. In this case, they seem to be due to intrinsic voids related with a reordering of lithium and niobium ions in the of oxygen sub-lattice with neutrally charged defects induced by their valence and ionic radii as confirmed by the Raman

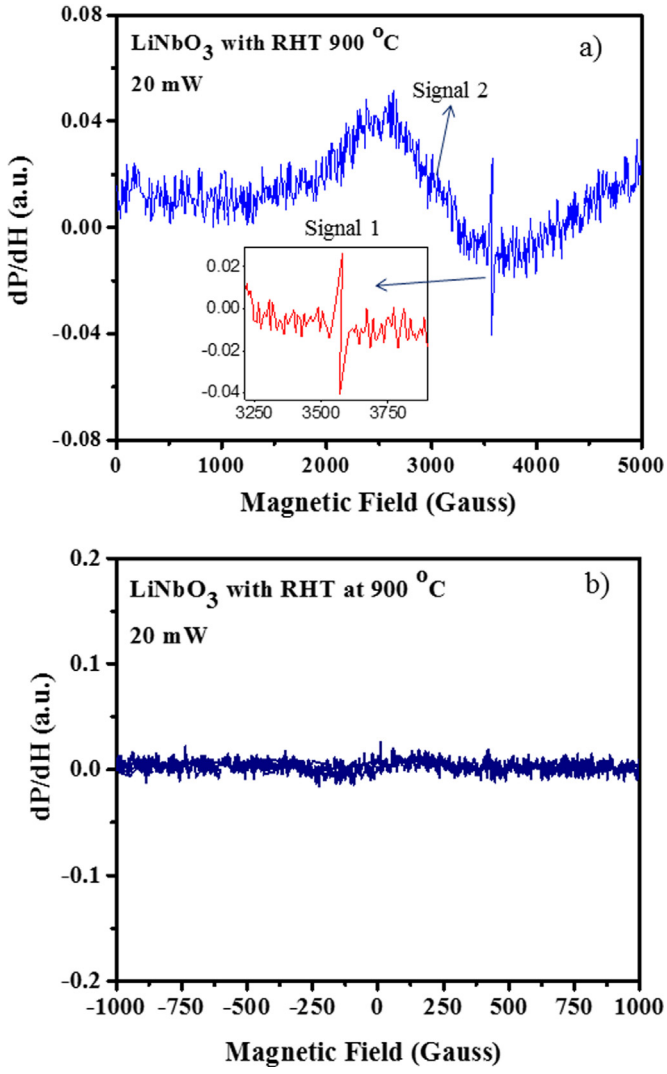

Fig. 6. (a) EPR signal (d*P*/d*H* vs magnetic field) at room temperature 300 K for representative $LiNbO_3$ with RHT at 900 °C; (b) the low-field microwave absorption (LFMA) spectra (d*P*/d*H* vs magnetic field, around zero field) at 300 K.

experiments. Fig. 6(b) shows the results for the low-field microwave absorption (LFMA) spectra (dP/dH vs magnetic field, around zero field) at 300 K for $LiNbO_3$ in representative samples subjected to RHT at 900 °C. The curve has a linear behavior with no slope and, also, it does not show hysteresis. Such behavior is different from superparamagnetism, where the isothermal measurement shows no hysteretic effects when taken at different temperatures, and of course in that case if the particle is small than the wall thickness there is no hysteresis and the different measurements will be superpose when plotted as function of *H*/*T* Diaz et al. [16]. This absorption is characteristic of paramagnetic samples and also tends to form nanoparticles clusters in agreement with Alvarez et al. [15] as confirm by STEM images.

3.5. Magnetocapacitance effect

It is found the dielectric constant increases when an external magnetic field is applied to $LiNbO_3$ nanoparticles subjected to RHT. This is evidence of a magneto capacitance coupling between ferroelectric and ferromagnetic domains, which were produced by inducing voids and defects into surface of nanoparticles. This was found before just from the ferromagnetic measurements [10,16]. Mangalam et al. [22] and Wang et al. [23], reported a magnetocapacitance effect in ferroelectric $BaTiO_3$ and $BiFeO_3$ respectively. Magnetocapacitive effect is defined in terms of the dielectric constant as follows:

$$(\mathrm{ME}) = \Delta\epsilon_r(H)/\epsilon_r(0) = [\epsilon_r(H) - \epsilon_r(0)]/\epsilon_r(0) \quad (2)$$

We have used capacitive measurements applying a magnetic field which was varied from 1 to ±30 kOe. Measurements are made at room temperature and at nine different frequencies ranging from 50 Hz to 1 MHz. Fig. 6(a) shows a sketch of set up samples respect to the magnetic field applied. The capacitive impedance is directly measured with the LRC meter and the capacitance is calculated from the well-known relation:

$$\chi_c = 1/2\pi fC \quad (3)$$

Samples without RHT has a constant value for the capacitance independent of the applied magnetic field of Cp=4.36 pF which is the same as the one reported for $LiNbO_3$ by Volk et al. [24]. Then, assuming a parallel plate configuration the dielectric constant is easily calculated with the dimension parameters mentioned before, and the results are displayed in the graphs of Fig. 7(b) and (c) for the samples with RHT at 650 °C, 900 °C and with RHT respectively. In these figures are observed the polarization mechanism in $LiNbO_3$ (black plot without interaction of magnetic field), when applied magnetic field from 1 to 30 kOe. It produces a conduction process and is mainly because of simultaneous presence of ferroelectric and ferromagnetic domains on crystallographically equivalent sites (red plot). Coupling magnetocapacitance has a local magnetic moment **m** may be represented by a charge that dynamically traces an orbit and a local dipole. Moment **p** may be represented by a positive point charge that lies asymmetrically within a crystallographic unit cell as shows in the graphs by represented green boxes (see Fig. 7(c) [3].This charge at higher frequencies does not follow the alternating field which results in an increase of κ-dielectric constant from 822 to 847 for the sample with RHT a 650 °C and from 822 to 860 for the sample treated a 900 °C evidence of magnetocapacitance coupling in $LiNbO_3$ nanoparticles. An explanation to determine an increasing of dielectric constant could be attributed to a polarization of due to external magnetic field, primarily at *d*-orbital as described by Mangalam et al. [22]. It was possible to calculate using Eq. (2), the magneto capacitance percentage in presence of external magnetic field of −30 to 30 kOe for the samples with RHT at 650 °C and 900 °C. The Fig. 7(d) shows the behavior of the magneto capacitance as a function of external magnetic field. In this figure we can see values of 2.3% and 3.2% for the samples with RHT at 650 °C and 900 °C respectively. This increase can be explained due to paraelectric ion Nb^{+4}, which is in symmetric position at octahedral of NbO_6 at $LiNbO_3$ framework, as presented in XPS and Raman spectroscopy. The process of magnetocapacitance is an indirect way of investigating the magnetoelectric coupling in multiferroic samples since an applied magnetic field not only affects the magnetic order, but also alters the dielectric constant of magnetoelectric materials [25]. The behavior of the magneto capacitance as a function of external magnetic field indicate that there is a low coupling in multiferroic due to not lineal behavior [25]. The percentage in the sample treated at 900 °C is higher than at 650 °C, because the magnetic materials in the shell of the nanoparticles is more effective, caused by the oxygen vacancies (see Fig. 2). Our previous work the Density functional theory was used to perform spin polarized electronic structure calculations for $LiNiO_3$ with and without oxygen vacancies per unit cell, the calculated magnetic moment is zero, regardless of where the vacancy was generated. With two oxygen vacancies it is possible to generate a non-zero magnetic moment, with a value close to 2 μ_B per unit cell, but only for certain specific combinations of vacancies [16].

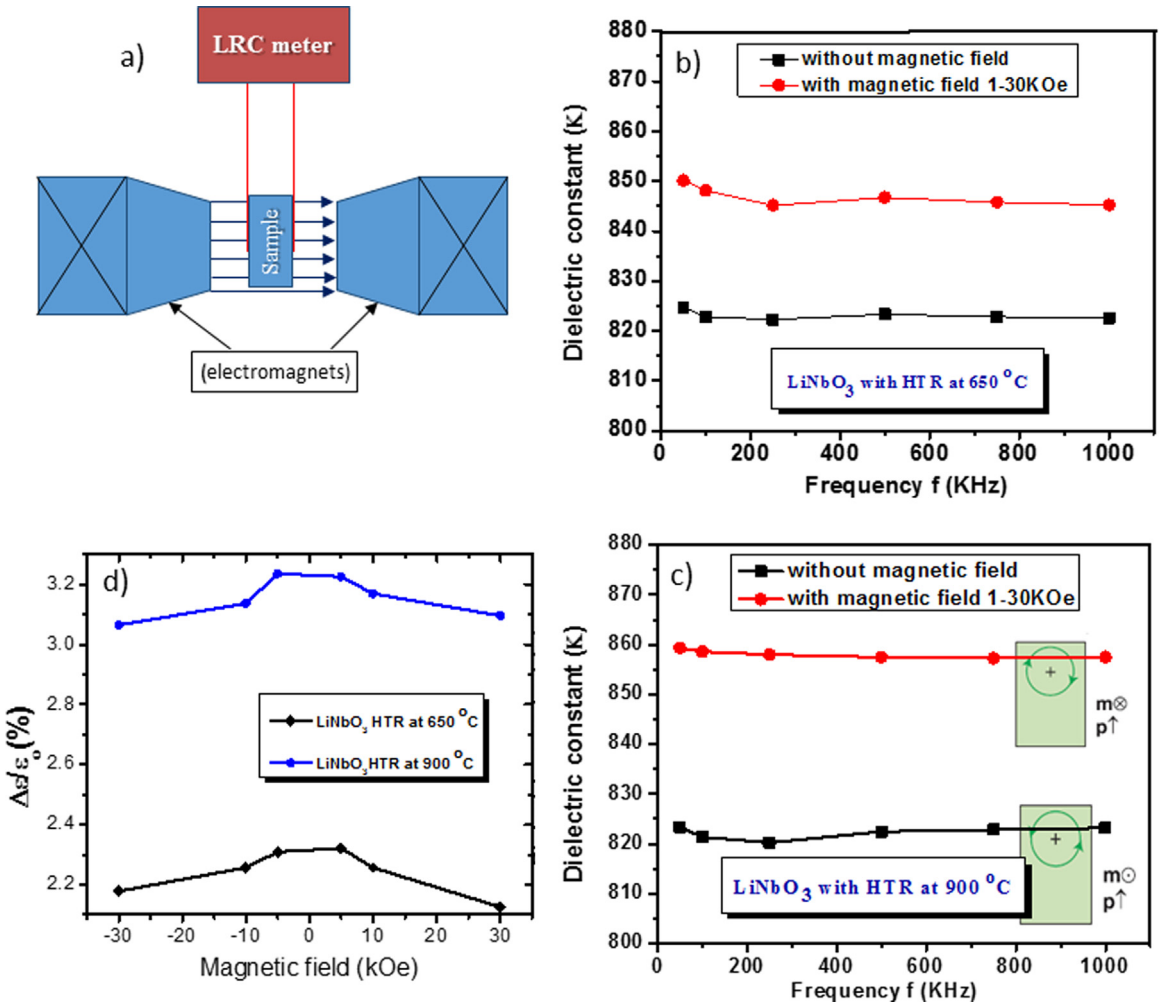

Fig. 7. (a) Sketch of the set up for magnetocapacitance measurements in $LiNbO_3$ nanocrystals without and with RHT; (b) and (c) polarization mechanism in $LiNbO_3$ (black plot) and magnetocapacitance coupling in ferromagnetic $LiNbO_3$ nanoparticles when applied magnetic field (red plot); (d) percentage of magnetocapacitive effect in ferromagnetic $LiNbO_3$ nanoparticles for samples at 600 °C and 900 °C respectively. (For interpretation of the reference to color in this figure legend, the reader is reffered to the web version of this article.)

4. Conclusions

There is an effect of the magnetocapacitance caused by the presence of magnetic moments in the shells of the $LiNbO_3$ nanocrystals created by the oxygen vacancies, structural defects Li/Nb and Nb^{+3}, $Nb^{+4}$and Nb^{+5} ions behavior during a heat treatment reduction process observed from Raman, electron paramagnetic resonance spectroscopy, and X-ray photoelectron spectroscopy analysis. There is also an increase of the intrinsic dielectric constant (κ) from 822 to 860 of for the optimum sample with treated at 900 °C by the magnetic field applied. The observed values of dielectric constant, magnetization and magnetocapacitive coupling may be useful for electronic devices application.

Conflicts of interest

All contributing authors declare no conflict of interest.

Acknowledgments

The authors want to thank Consejo Nacional de Ciencia y Tecnologia-México for economical support through Postdoctoral Abroad Program, Solicitation #250381. This work was supported by CONACyT project 129293, DGAPA-UNAM project IN106014, BISNANO, and ICYTDF, project PICCO. Thanks to J. Morales, A. Lopez, R.P. Talamantes for help in computational and technical problems, and to F. Silvar for He provisions.

References

[1] M.J. Fiebig, Revival of the magnetoelectric effect, J. Phys. D: Appl. Phys. 38 (2005) 123–152.
[2] N.A. Sapalding, M. Fiebig, The renaissance of magnetoelectric multiferroics, Science 309 (2005) 309–391.
[3] W. Eerenstein, N.D. Mathur, J.F. Scott, Multiferroic and magnetoelectric materials, Nature 442 (2006) 759–765.
[4] J.M.D. Coey, P. Stamenov, R.D. Gunning, M. Venkatesanand, K. Paul, Ferromagnetism in defect-ridden oxides and related materials, New J. Phys. 12 (2010) 14.
[5] R.S. Weis, T.K. Gaylord, Lithium niobate: summary of physical properties and crystal structure, Appl. Phys. 37 (1985) 191–203.
[6] Y. Kong, S. Liu, J. Xu, Recent advances in the photorefraction of doped lithium Niobate crystals, Materials 5 (2012) 1954–1971.
[7] C. Song, F. Zeng, Y.X. Shen, K.W. Geng, Y.N. Xie, Z.Y. Wu, F. Pan, Local Co structure and ferromagnetism in ion-implanted Co-doped $LiNbO_3$, Phys. Rev. B 73 (2006).
[8] T. Kimura, S. Kawamoto, I. Yamada, M. Azuma, M. Takano, Y. Tukura, Magnetocapacitance effect in multiferroic $BiMnO_3$, Phys. Rev. B 67 (2003).
[9] J. Hemberger, P. LunKenheimer, R. Fichtl, H.A. Krug von Niddia, V. Tsurkan, A. Loidl, Relaxor ferroelectricity and colossal magnetocapacitive coupling in ferromagnetic $CdCr_2S_4$, Nature 434 (2005) 364–367.
[10] C. Díaz-Moreno, R. Farias, A. Hurtado-Macias, J. Elizalde-Galindo, J. Hernandez-

Paz, Multiferroic response of nanocrystallinelithiumniobate, J. Appl. Phys. 111 (2012).
[11] P.S. Dobal, R.S. Katiyar, Studies on ferroelectric perovskites and Bi-layered compounds using micro-Raman spectroscopy, J. Raman Spectrosc. 33 (2002) 405–423.
[12] G. Alvarez, R. Font, J. Portelles, R. Valenzuela, Electron paramagnetic resonance study of the ferroelectromagnet $Pb(Fe_{1/2}Nb_{1/2})O_3$ through ferro-paraelectric transition, Mater. Lett. 62 (2008) 1737–1739.
[13] G. Alvarez, R. Font, J. Portelles, R. Valenzuela, R. Zamorano, Signature of weak ferromagnetism by electron paramagnetic resonancein the ferroelectro-magnet $Pb(Fe_{1/2}Nb_{1/2})O_3$, Physica B 384 (2006) 322–325.
[14] G. Alvarez, H. Montiel, J.F. Barron, M.P. Gutierrez, R. Zamorano, Yafet–Kittel-type magnetic ordering in $Ni_{0.35}Zn_{0.65}Fe_2O_4$ ferrite detected by magneto-sensitive microwave absorption measurements, J. Magn. Magn. Mater. 322 (2010) 348–352.
[15] G. Alvarez, J.A. Peña, M.A. Castellanos, H. Montiel, R. Zamorano, A microwave absorption study in the ferromagnetoelectric $Pb(Fe_{1-x}M_x)O_3$ (M=Ta, W, Nb) perovskites, Rev. Mex. Fís. 58 (2012) 24–27.
[16] C.A. Díaz-Moreno, R. Farías-Mancilla, J.A. Matutes-Aquino, J. Elizalde-Galindo, F. Espinosa-Magaña, J. González-Hernández, A. Hurtado-Macías, Magnetic behavior in $LiNbO_3$ nanocrystallites caused by oxygen vacancies, J. Magn. Magn. Mater. 356 (2014) 82–86.
[17] C.A. Diaz-Moreno, R. Farias-Mancilla, J. González-Hernández, A. Hurtado-Macias, D. Bahena, M.J. Yacamán, M. Ramos, Structural aspects $LiNbO_3$ nano-particles and their ferromagnetic properties, Materials 7 (2014) 7217–7225.
[18] Y. Repelin, E. Husson, F. Bennani, C. Proust, Raman spectroscopy of lithium niobate and lithium tantalate. Force field calculations, J. Phys. Chem. Solids 60 (1999) 819–825.
[19] K.L. Sweeney, L.E. Halliburton, Oxygen vacancies in lithium niobate, Appl. Phys. Lett. 43 (1983) 336–338.
[20] K. Tabata, M. Kamada, T. Choso, H. Munakata, Photoelectron spectroscopy investigation of NO adsorption on defects of $LiNbO_3$ surfaces, Appl. Surf. Sci. 125 (1998) 93–98.
[21] R. Courths, P. Steiner, H. Höchst, S. Hüfner, Photoelectron-spectroscopy investigation and electronic properties of $LiNbO_3$ crystal surfaces, Appl. Phys. 21 (1980) 345–352.
[22] R.V.K. Mangalam, N. Ray, U.V. Waghmare, A. Sundaresan, C.N.R. Rao, Multiferroic properties of nanocrystalline $BaTiO_3$, Solid State Commun. 149 (2009) 1–5.
[23] D.H. Wang, W.C. Goh, M. Ning, C.K. Ong, Effect of Ba doping on magnetic, ferroelectric, and magnetoelectric properties in mutiferroic $BiFeO_3$ at room temperature, Appl. Phys. Lett. 88 (2006).
[24] T. Volk, M. Wöhlecke, Lithium Niobate: Defects, Photorefraction and Ferroelectric Switching, Springer-Verlag, Berlin, 2008.
[25] G. Catalan, Magnetocapacitance without magnetoelectric coupling, Appl. Phys. Lett. 88 (2006).